A missing link in the carbon cycle: phytoplankton light absorption under RCP emissions scenarios

Rémy Asselot[1,*], Philip Holden[2], Frank Lunkeit[3], and Inga Hense[1]

[1]Institute for Marine Ecosystem and Fishery Science, Center for Earth System Research and Sustainability, University of Hamburg, Hamburg, Germany
[2]Environment, Earth and Ecosystems, The Open University, Walton Hall, Milton Keynes, MK7 6AA, UK
[3]Meteorological Institute, Center for Earth System Research and Sustainability, University of Hamburg, Hamburg, Germany
[*]Now at University of Brest, Ifremer, CNRS, IRD, Laboratoire d'Océanographie Physique et Spatiale (LOPS), F-29280, Plouzané, France.

Correspondence: Rémy Asselot (remy.asselot@ifremer.fr)

Abstract. Marine biota and biogeophysical mechanisms, such as phytoplankton light absorption, have attracted increasing attention in recent climate studies. Under global warming, the influence of phytoplankton on the climate system is expected to change. Previous studies analyzed the impact of phytoplankton light absorption under prescribed future atmospheric CO_2 concentrations. However, the role of this biogeophysical mechanism under freely-evolving atmospheric CO_2 concentration and future CO_2 emissions remains unknown. To shed light on this research gap, we perform simulations with the EcoGEnIE Earth system model and prescribe CO_2 emissions out to 2500 following the four Extended Concentration Pathways (ECP) scenarios, which for practical purpose we call RCP scenarios. Under all RCP scenarios, our results indicate that phytoplankton light absorption leads to a shallower remineralization of organic matter and a reduced export efficiency, weakening the biological carbon pump. In contrast, this biogeophysical mechanism increases the surface chlorophyll, the sea surface temperature, the atmospheric CO_2 concentrations and the atmospheric temperature. Under the RCP2.6, RCP4.5 and RCP6.0 scenarios, the magnitude of changes due to phytoplankton light absorption is similar. However, under the RCP8.5 scenario, the changes in the climate system are less pronounced due to decreasing ecosystem productivity as temperature increases, highlighting a reduced effect of phytoplankton light absorption under strong warming. Additionally, this work highlights the major role of phytoplankton light absorption on the climate system, suggesting highly uncertain feedbacks on the carbon cycle with uncertainties that maybe in the range of those known from the land biota.

1 Introduction

Under anthropogenic climate change, observations indicate that the future changes of phytoplankton biomass and net primary production are highly uncertain. For instance, satellite observations demonstrate that low-latitude oceans have become greener due to climate change between 2002-2022 (Cael et al., 2023). In contrast, oceanographic measurements from 1890 to 2010 reveal that chlorophyll concentration has declined over more than 62% of the ocean surface (Boyce et al., 2014). Additionally, Polovina et al. (2008) indicate that between 1998 and 2006, low surface chlorophyll areas have expanded by 15% on a

global scale although their results might not be exclusively attributed to climate change due to their short time series (Henson et al., 2010; Schlunegger et al., 2020). Using an ocean-color database spanning 6 years, McClain et al. (2004) show that the oligotrophic waters expand in the Northern hemisphere while the expansion in the Southern hemisphere is much weaker.

25 Complementing these observations, modeling studies have also investigated the future changes in net primary production due to anthropogenic warming. For instance, on a global scale, a CMIP6 model-ensemble study indicates a decrease in depth-integrated net primary production of 2.99±9.11% by the end of the 21st century under the high emission scenario SSP5-8.5 (Kwiatkowski et al., 2020). However, this estimate is rather imprecise due to incomplete understanding and insufficient observational constraints; thus the projections of net primary production changes show large uncertainties (Tagliabue et al., 2021).

30 On a regional scale, projected changes in primary production are also uncertain. For instance, in the Mediterranean Sea, Richon et al. (2019) show a decline in net primary production of 10% in the 2090s under the high-emission SRES-A2 scenario. However, in the same basin, Reale et al. (2022) demonstrate that, under the RCP4.5 and RCP8.5 scenarios, the net primary production increase is greater than 10 gC/m^2/yr by the end of the 21st century. These conflicting results come from the different parameterizations adopted which exert differing influences of temperatures on simulated net primary production. These

35 changes in primary production, phytoplankton abundance, distribution and biogeography have consequently an impact on the role of phytoplankton light absorption.

Different modeling studies investigate the effect of phytoplankton light absorption on the oceanic temperature under global warming. It is suggested that the decrease in phytoplankton abundance will increase ocean clarity and lead to a lower biolog-

40 ical increase of sea surface temperature (SST). A reduction of phytoplankton-induced oceanic warming could thus counteract in part the warming associated with climate change (Patara et al., 2012). To study the effect of phytoplankton light absorption in a warming scenario, Sonntag (2013) modified the oceanic forcing by increasing the sea surface temperature for the whole model domain by 3°C. Taking into account phytoplankton light absorption, surface phytoplankton concentrations are enhanced and the maximum SST increase is 0.4°C compared to a present-day scenario (Sonntag, 2013). Furthermore, Paulsen (2018)

45 uses an Earth system model of high complexity to perform simulations under a transient increase of 1% of atmospheric CO_2 per year. With phytoplankton light absorption, Paulsen (2018) reports a decline in chlorophyll concentrations and an enhanced circulation in the upwelling regions, leading to a local oceanic warming of up to 0.7°C. Additionally, the sensitivity of the light attenuation coefficient for phytoplankton is investigated under the RCP8.5 scenario (Kvale and Meissner, 2017). Depending on the parameterization choice, the authors highlight that phytoplankton light absorption may reduce or increase net primary

50 production between 1800 and 2100. Additionally, using a coupled ocean-atmosphere model, Park et al. (2015) focus on the Arctic region to study phytoplankton light absorption under global warming. They conduct simulations where atmospheric CO_2 concentration increases by 1% per year from the level of 1990 to double its initial concentration. The authors show that phytoplankton light absorption amplifies future Arctic warming by 20%. All these previous studies have demonstrated that phytoplankton light absorption affects the future climate projections but, to this day, this biogeophysical mechanism is missing

55 from 50% of the CMIP6 models (Pellerin et al., 2020).

To date, the impact of phytoplankton light absorption on oceanic temperature under oceanic warming (Sonntag, 2013), constant atmospheric CO_2 concentration (Patara et al., 2012) and prescribed rising atmospheric CO_2 concentrations (Park et al., 2015; Kvale and Meissner, 2017; Paulsen, 2018) has been investigated. However, Asselot et al. (2022) study how atmospheric temperature is affected by phytoplankton light absorption. To do so, the authors compare the changes in air-sea heat versus air-sea CO_2 exchange due to this biogeophysical mechanism. They conclude that phytoplankton light absorption mainly affects the climate system via air-sea CO_2 exchange. Therefore, prescribing atmospheric CO_2 concentrations for global warming simulations blurs the real effect of this biogeophysical mechanism. The purpose of this study is to better understand how phytoplankton light absorption will be affected by anthropogenic climate change via changes in phytoplankton biomass and distribution. To address this question, we performed simulations with and without phytoplankton light absorption in experiments with prescribed atmospheric CO_2 emissions. We are interested in long-term climate effects and so we applied the intermediate complexity Earth system model EcoGEnIE (Ward et al., 2018). We force the model with atmospheric CO_2 emissions out to 2500 following the four Extended Representative Concentration Pathways (RCP) scenarios used by the Intergovernmental Panel on Climate Change (IPCC) for their Fifth Assessment Report (Moss et al., 2010).

2 Methods

The Earth System model (ESM) used in this study is called EcoGEnIE (Ward et al., 2018) and is a coupling between a new ecosystem component (ECOGEM) and cGEnIE (Ridgwell et al., 2007). EcoGEnIE is an ESM of intermediate complexity (EMIC) (Claussen et al., 2002) and due to the limitations of such a model, we focus on the quantification of the large-scale impacts of phytoplankton light absorption but we do not quantify the components or drivers of those large-scale impacts. We chose to conduct our study with an EMIC because we are interested on the effect on particular climate mechanism (e.g. phytoplankton light absorption) and it would have been difficult to isolate this effect with an ESM of high complexity, due to numerous climate feedbacks implemented in high complexity ESM. Moreover, cGEnIE is widely used to study past climate systems and the carbon cycle over geological timescales (Gibbs et al., 2016; Meyer et al., 2016; Greene et al., 2019; Stockey et al., 2021). EcoGEnIE was already used to analyze the role of marine phytoplankton in the warm early Eocene period (Wilson et al., 2018) and to explore the relationships between plankton size, trophic complexity and the availability of phosphorus during the late Cryogenian (Reinhard et al., 2020). We use the same configuration as described in Asselot et al. (2021). This model contains components that represent climate processes, including ocean dynamics, marine biogeochemistry, marine ecosystem, atmospheric circulation and sea-ice dynamics (Figure 1). We do not consider a dynamical land scheme and neglect the terrestrial carbon cycle. For this study, we modify the ecosystem component and the oceanic component to implement phytoplankton light absorption.
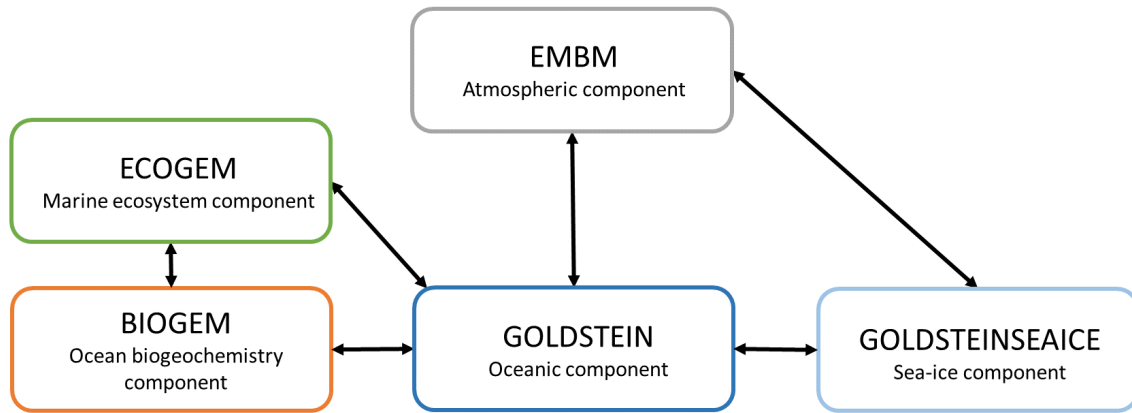
Figure 1. Sketch representing the different components of the EcoGEnIE model. Black arrows represent the links between the different components. GEnIE is controlled by a bespoke coupling manager which was developed for user-friendly modularity and flexibility, so that, for instance the EMBM atmosphere can be replaced with a fully dynamic 3D atmosphere PLASIM (Holden et al., 2016) via a single switch in the model configuration file. Figure from Asselot et al. (2022).

2.1 Ocean, atmosphere and sea-ice representation

The oceanic component is a 3D frictional-geostrophic oceanic component (GOLDSTEIN) that calculates the horizontal and vertical redistribution of heat, salinity and biogeochemical elements (Edwards and Marsh, 2005). The horizontal grid (36×36) is uniform in longitude and uniform in sine latitude, giving $\sim 3.2°$ latitudinal increments at the equator increasing to $19.2°$ in
90   the polar regions. This horizontal grid has been employed as the standard resolution to study the global carbon cycle (Cameron et al., 2005). Furthermore, we consider 32 vertical oceanic layers, increasing logarithmically from 29.38 m for the surface layer to 456.56 m for the deepest layer. The model underestimates the upwelling in the northeastern Atlantic, Arabian Sea and polar regions (Ward et al., 2018). In contrast, Ridgwell et al. (2007) indicate that the low-latitude upwelling in the Western Equatorial Pacific and Equatorial Indian Ocean give an excess of phosphate of 0.5 μmol/kg compared to observations (Conkright and
95   Levitus, 2002). However, on a global scale, Marsh et al. (2011) show that the model simulates realistic upwelling.
The atmospheric component (EMBM) is closely based on the UVic Earth system model (Weaver et al., 2001). It is a 2D model, where atmospheric temperature and specific humidity are the prognostic variables. Heat and moisture are horizontally transported by winds and mixing. The incoming shortwave radiation at the top of the atmosphere depends on the planetary albedo, which varies as a function of latitude and time of year to account for the effects of changes in solar zenith angle.
100   The net longwave radiation represents $\sim 45\%$ of the total atmospheric energy balance while net shortwave radiation represents $\sim 25\%$. The radiative forcing associated with changes in atmospheric CO_2 concentrations is considered in the calculation of outgoing planetary longwave (Q_{PLW}). Higher atmospheric CO_2 concentration leads to higher amount of Q_{PLW} being trapped in the atmosphere. Furthermore, the parameterization for Q_{PLW} is taken from Thompson and Warren (1982) and depends on the surface relative humidity and atmospheric temperature through a logarithmic dependency. Precipitation instantaneously

removes all moisture corresponding to the excess above a relative humidity threshold. Wind velocities are prescribed following the annual average data of Trenberth (1989) and a constant and dimensionless land surface drag coefficient is set to 1×10^{-3} (Weaver et al., 2001).

The sea-ice component (GOLDSTEINSEAICE) solves the fraction of the ocean surface covered by ice within a grid cell and computes the average sea-ice thickness (Edwards and Marsh, 2005). A diagnostic equation is solved for the ice surface temperature. The growth or decay of sea ice depends on the net heat flux into the ice (Hibler, 1979; Semtner, 1976). Sea-ice dynamics consists of advection by surface currents and diffusion. The sea-ice component acts as a coupling module between the ocean and the atmosphere, where heat and freshwater are exchanged and conserved between these three modules.

2.2 Ocean biogeochemistry component

The biogeochemical module (BIOGEM) represents the transformation and spatial redistribution of biogeochemical tracers (Ridgwell et al., 2007). The state variables are inorganic nutrients and organic matter. Organic matter is partitioned into dissolved and particulate organic matter (DOM and POM). The model includes iron (Fe) and phosphate (PO_4) as limiting nutrients. Similar to Asselot et al. (2021), we do not explicitly consider nitrate (NO_3^-) but approximate it through the N:P Redfield ratio of 16:1 (Ridgwell et al., 2007). Furthermore, BIOGEM calculates the air-sea CO_2 and O_2 exchange. These fluxes depend on the gas transfer velocity, the water density, the concentration of dissolved gas in the ocean surface, the solubility coefficient calculated from Wanninkhof (1992), the concentration of gas in the atmosphere, and the fraction of the ocean covered by sea ice (Ridgwell et al., 2007).

2.3 Ecosystem community component

The marine ecosystem component (ECOGEM) represents the marine plankton community and associated interactions within the ecosystem (Ward et al., 2018). The biological uptake in ECOGEM is limited by light, temperature and nutrient availability. Phytoplankton are allowed to flexibly take up nutrients according to availability. The production of dead organic matter is a function of mortality and messy feeding. The surface production is then distributed along the water column as a depth-dependent flux. To achieve this, the flux is partitioned between POM, of which, on average 70% is remineralized below the euphotic layer (0 – 221.84 m), and DOM which is predominantly remineralized within this layer. In ECOGEM, the sinking speeds of organic matter are constant. The model assumes that photosynthesis is a Poisson function of irradiance and that phytoplankton growth is limited by this function (Geider et al., 1998; Moore et al., 2001). The phytoplankton growth model requires NO_3^- to simulate chlorophyll synthesis but we do not consider this nutrient in our study. As a consequence, the nitrate biomass is equal to the phosphate biomass multiplied by the standard Redfield ratio of 16 (Ward et al., 2018). Nutrient uptake is a Michaelis-Menten function and phytoplankton growth is limited by a minimum function of internal nutrient status. Plankton biomass and organic matter are subject to processes such as resource competition and grazing before being passed to DOM and POM. The ecosystem is divided into different plankton functional types (PFTs) with specific traits. Each PFT can be subdivided into size classes with specific size-dependent traits. Yet we incorporate only two PFTs: one phytoplankton and one zooplankton group. We consider only one phytoplankton and one zooplankton class size, following the low ecosystem

complexity model of Asselot et al. (2021), noting that Asselot et al. (2021) found that the climate impact of changing ecosystem complexity was negligible compared to that from phytoplankton light absorption. Phytoplankton is characterized by nutrient
140 uptake and photosynthesis whereas zooplankton is characterized by predation traits. Zooplankton grazing depends on the concentration of prey biomass and prey size, predominantly grazing on preys that are 10 times smaller than themselves. The model considers inorganic resources (DIC, PO_4 and Fe), plankton biomass and organic matter (POM and DOM) as state variables. Living matter is not subject to ocean transport. Communication between biological communities only occurs through the advection and diffusion of inorganic and non-living organic matter. This approximation is justified by the coarse model
145 resolution (∼1000 km) and limited transport range of living matter, so th rate of transport between grid cells is slow in relation to the net growth rates of plankton community (Ward et al., 2018). ECOGEM considers a dynamic photoacclimation (Geider et al., 1998) where the chlorophyll-to-carbon ratio is regulated as the cell attempts to balance the rate of light capture by chlorophyll with the maximum potential rate of carbon fixation. Phytoplankton biomass can only be lost via grazing and mortality. Plankton mortality is reduced at very low biomass such that plankton cannot become extinct. The production of
150 alkalinity is coupled to phytoplankton uptake of phosphate via a fixed linear ratio, meaning that alkalinity increases while phosphate is consumed. The exports of calcium carbonate ($CaCO_3$) and alkalinity are scaled to the export of POC via a spatially uniform value which is modified by a thermodynamically based relationship with the calcite saturation state. The dissolution of $CaCO_3$ below the surface is treated similarly to that of POM.

2.4 Temperature limitation

155 Metabolic processes of photosynthesis, nutrient uptake and zooplankton predation are all driven by the same exponential temperature limitation term (Ward et al., 2018). The temperature limitation scheme is given by Eq. 1:

$$\gamma_T = \exp(A \cdot (T - T_{ref})) \tag{1}$$

where γ_T is the temperature limitation, A is the temperature sensitivity ($0.05°C^{-1}$), T is the sea surface temperature and T_{ref} is the reference temperature. A reference temperature of 20°C is used because most experimentally determined metabolic rates
160 are made at this temperature (Behrenfeld and Falkowski, 1997; Goldman, 1977; Rhee and Gotham, 1981). Photosynthesis is light limited, which results in a sub-exponential growth rate, while competing effects of nutrient demand and zooplankton predation increase exponentially and together progressively limit net productivity as temperatures increase. We note that temperature dependence may be complicated by co-varying factors such as nutrient availability, leading to disproportionate effects depending on location. To explore these dependencies, chlorophyll and nutrient density are plotted against SST in appendices
165 A1 and A2 respectively, with data separated into binned subsets with different nutrient density. When nutrient density is low (< 0.017 mmol/m³), 30% of the variance in chlorophyll is explained by temperature, with a negligible contribution of co-varying nutrient (only 7% of nutrient variance can be explained by SST in this bin). In contrast, under high nutrient concentrations (>0.1 mmol/m³), while 51% of the variance in chlorophyll can be explained by temperature, as much as 41% of this could be explained by co-variance of nutrients with temperature. In summary chlorophyll is limited by increasing temperature both

170   through increased nutrient demand and zooplankton grazing, and through reduced nutrient availability, likely, at least in part, driven by the increasing nutrient demand.

2.5   Phytoplankton light absorption

In the original model version (Ward et al., 2018), light was only absorbed by phytoplankton. Following Asselot et al. (2021), a new light scheme is implemented where the absorbed light by phytoplankton is converted into heat and is able to affect

175   the oceanic temperature. In the current model configuration, the incoming shortwave radiation varies seasonally. Moreover, the light level is calculated as the mean level of photosynthetically available radiation within each oceanic layer. The light penetrates until the sixth oceanic layer of the model (221.84 m), representing the base of the euphotic zone. The maximum light absorption occurs in the surface layer while the minimum absorption happens in the sixth layer. The propagation of light within the ocean is limited by pure water and chlorophyll cells (Ward et al., 2018). The vertical light attenuation scheme is

180   given by Eq. 2:

$$I(z) = I_0 \cdot \exp(-k_w \cdot z - k_{Chl} \cdot \int_0^z Chl(z) \cdot dz) \tag{2}$$

where $I(z)$ is the radiation at depth z, I_0 is the radiation at the surface of the ocean, k_w is the light absorption by clear water (0.04 m^{-1}), k_{Chl} is the light absorption by chlorophyll (0.03 m^{-1}(mg Chl)$^{-1}$) and $Chl(z)$ is the chlorophyll concentration at depth z. The values for k_w and k_{Chl} are taken from Ward et al. (2018). The parameter I_0 is negative in the model because

185   it is a downward flux from the sun to the surface of the ocean. Phytoplankton changes the optical properties of the ocean through phytoplankton light absorption, causing radiative heating and changing the heat distribution in the water column (e.g. Wetzel et al., 2006; Anderson et al., 2007; Sonntag, 2013). We implement phytoplankton light absorption into the model (Eq. 3) following the scheme of Hense (2007) and Patara et al. (2012):

$$\frac{\partial T}{\partial t} = \frac{1}{\rho \cdot c_p} \frac{\partial I}{\partial z} \tag{3}$$

190    $\partial T / \partial t$ denotes the water temperature change only associated with radiative heating, c_p is the specific heat capacity of water, ρ is the ocean density, I is the solar radiation incident at the ocean surface, and z is depth. We assume that the whole light absorption heats the water (Lewis et al., 1983).

2.6   The Representative Concentration Pathways scenarios

The RCP scenarios include the temporal evolution of greenhouse gas emissions into the atmosphere (Moss et al., 2010). Origi-

195   nally, there were four RCP scenarios, namely RCP2.6, RCP4.5, RCP6.0 and RCP8.5 (Figure 2), labeled after a net enhancement of radiative forcing at the beginning of the 22nd century (2.6, 4.5, 6.0 and 8.5 W/m^2, respectively). These scenarios are consistent with socio-economic assumptions and associated greenhouse gas emissions. They comprise a stringent mitigation scenario

(RCP2.6), two intermediate scenarios (RCP4.5 and RCP6.0) and a high greenhouse gas emissions scenario (RCP8.5). The RCP scenarios only span the 2005-2100 period but this study is conducted on a multi-century timescale to understand the long-term climate response. As a consequence, our study requires data beyond 2100. We therefore use the Extended Concentration Pathways (ECPs) designed by stakeholders and scientific groups and spanning the 2100-2500 period (Meinshausen et al., 2011). Similar to RCP2.6, ECP2.6 represents a strong mitigation scenario including negative CO_2 emissions from 2100 to 2500. For ECP4.5 and ECP6.0, the atmospheric CO_2 emissions start to decrease in the 21st century while for ECP8.5 this decrease happens at the end of the 22nd century. For practical purposes, here, referring to the RCP scenarios indicates the period between 1765 and 2500. We consider a multi-century timescale to evaluate the long term influence of anthropogenic CO_2 emissions. Even if these emissions cease or are reduced by 2100, their influence will be echoed for centuries.
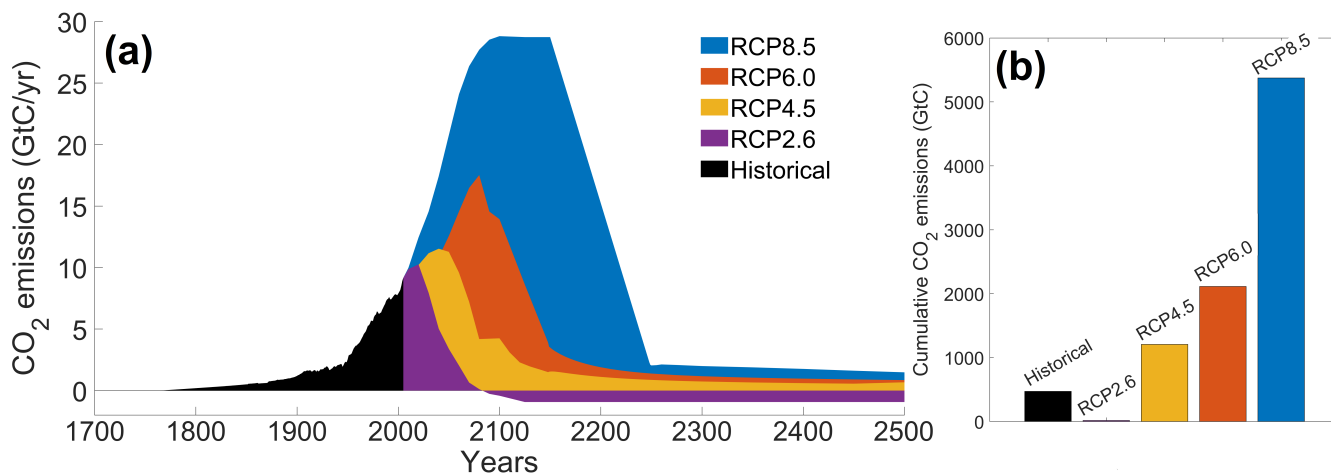
Figure 2. Atmospheric CO_2 emissions following the RCP scenarios. (a) Historical and scenarios of future CO_2 emissions over time (GtC/yr). (b) Cumulative CO_2 emissions for the different scenarios (GtC). The historical emissions represent the cumulative CO_2 emissions from 1765 to 2005. The RCP scenarios represent the cumulative CO_2 emissions between 2006 and 2500. The color coding between the two panels is identical.

2.7 Model setup and simulations

We use the same model setup and parametrization as described in Asselot et al. (2021), with 32 oceanic vertical layers, net primary production allowed until the sixth vertical layer (221.84 m deep) and incoming shortwave radiation varying seasonally. The ecosystem community is consistent with the community described in Asselot et al. (2021), with one phytoplankton group and one zooplankton group (Appendix B1). First, we run a 10,000 years spin-up with only BIOGEM to achieve a realistic distribution of nutrients. The spin-up is run with a constant pre-industrial atmospheric CO_2 concentration of 278 ppm. Second, ECOGEM is switched on and the simulations are run for 736 years, representing the period between 1765 and 2500 (Meinshausen et al., 2011). Switching on ECOGEM has an impact on the biogeochemistry via a different uptake of nutrients and carbon. However, we are interested in the effect of light absorption by phytoplankton relative to simulations without light

absorption and our experimental results are differences between two otherwise identical simulations; the altered atmospheric CO_2 and subsequent long-term drift in the carbon cycle induced by ECOGEM are common to both experiments. In total we run 8 simulations with historical runs between 1765-2005 followed by RCP scenarios for the period between 2006 and 2500. The simulations are run with and without phytoplankton light absorption (Table 1). For the simulations without phytoplankton light absorption $k_{Chl} = 0$ m^{-1}(mg Chl)$^{-1}$ meaning that light is only attenuated by k_w (Eq. 2). We run the simulations with prescribed global CO_2 emissions, which are the sum of the fossil, industrial and land-use related CO_2 emissions (Figure 2). Moreover, all simulations include ECOGEM and are forced with the same constant flux of dissolved iron into the ocean surface (Mahowald et al., 2006). We compare the yearly-averaged outputs of the year 2500.

Table 1. Name and description of the simulations (PLA = phytoplankton light absorption).

Name	Description
RCP2.6	CO_2 emissions following RCP2.6
RCP2.6-LA	CO_2 emissions following RCP2.6 with PLA
RCP4.5	CO_2 emissions following RCP4.5
RCP4.5-LA	CO_2 emissions following RCP4.5 with PLA
RCP6.0	CO_2 emissions following RCP6.0
RCP6.0-LA	CO_2 emissions following RCP6.0 with PLA
RCP8.5	CO_2 emissions following RCP8.5
RCP8.5-LA	CO_2 emissions following RCP8.5 with PLA

2.8 Model inter-comparison

To validate our model setup, we compare our results with the results of an EMIC intercomparion (Zickfeld et al., 2013), which has a model setup close to our model setup. To be consistent with Zickfeld et al. (2013), we compute the surface atmospheric temperature (SAT) increase between the periods 1986-2005 and 2281-2300, without phytoplankton light absorption. Independently of the RCP scenario, Figure 3 shows that our increases in SAT are in agreement with the global mean warming of Zickfeld et al. (2013) and lie in between the model ensemble minimum and maximum values. Thus, our model setup is suitable to study climate change.
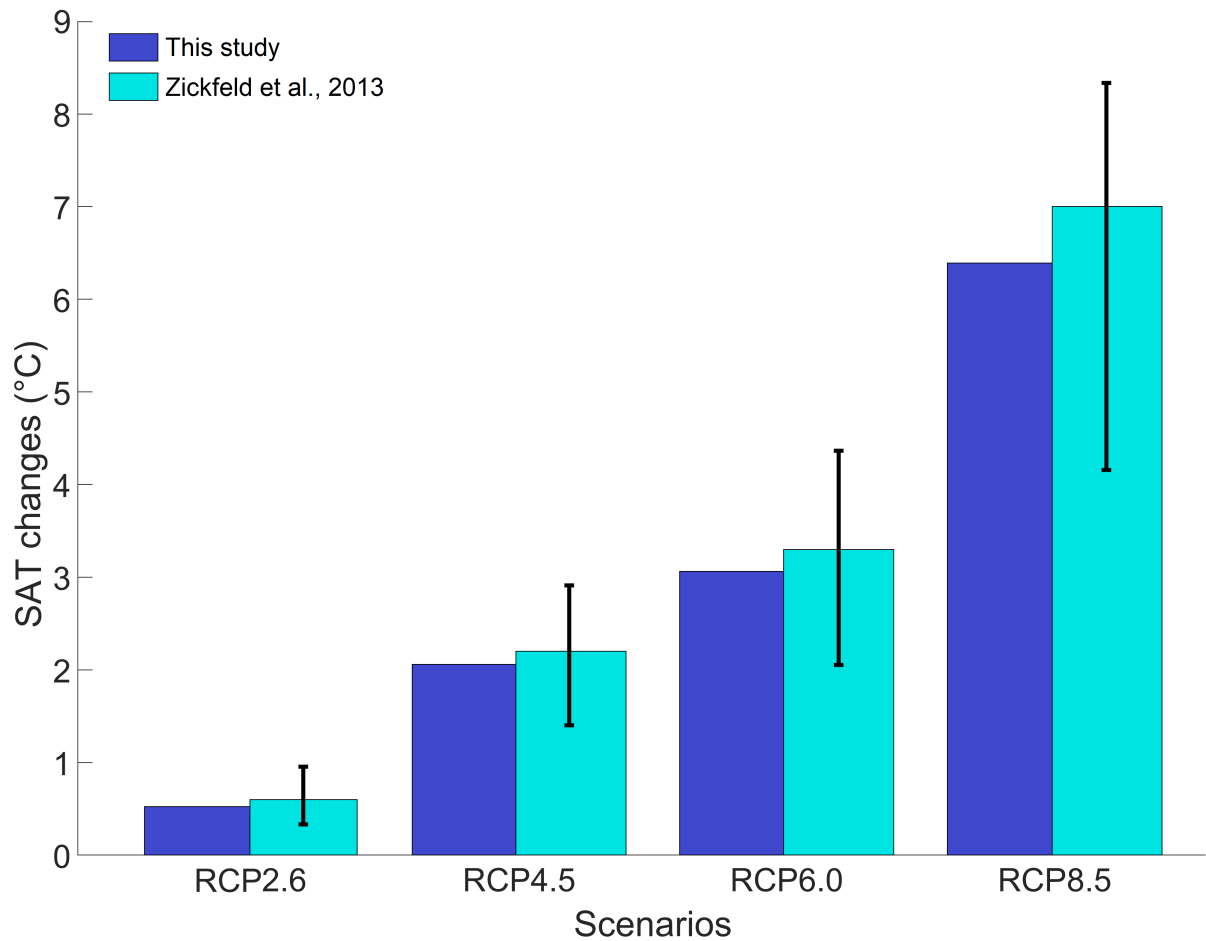
Figure 3. Global mean SAT changes (°C) between the periods 1986-2005 and 2281-2300 for our study (blue) and the study of Zickfeld et al. (2013) (turquoise). The black vertical lines represent the minimum and maximum values from the model inter-comparison of Zickfeld et al. (2013). The SAT changes of our study come from simulations without phytoplankton light absorption.

3   Results

In this section, we are interested in resolving the effects of phytoplankton light absorption and the relative differences between the simulations. Due to the limitations of such an EMIC, the absolute values are less relevant. We first look at ocean properties such as the biological pump, surface chlorophyll and SST. Second, we investigate the changes in atmospheric CO_2 concentrations and SAT.

235

3.1 Oceanic properties

3.1.1 The biological carbon pump

To compare the strength of the biological carbon pump between our simulations, we consider vertical fluxes of POC in the water column. In our study, these fluxes are described by an exponential decay, which is fixed and spatially invariant. Under RCP2.6,
240 RCP4.5 and RCP6.0 scenarios, the POC flux decreases by 4-5% when phytoplankton light absorption is simulated (Table 2). For the RCP8.5 scenario, the effect is smaller, with a POC flux reduced by 1% due to phytoplankton light absorption. In our simulations, independently of the RCP scenario, phytoplankton light absorption decreases the POC flux (Table 2), indicating that less organic matter is transported towards the bottom of the ocean. This reduced export efficiency is due to an enhanced remineralization at the ocean surface, which is driven by a higher amount of organic matter in the ocean surface. Indeed, the
245 surface net primary production increases with phytoplankton light absorption (Table 2), leading to an enhanced remineralization located in the surface layer of the ocean. These results indicate that biological pump is weaker with phytoplankton light absorption meaning that more inorganic matter, such as nutrients, is located in the surface of the ocean (Table D1).

Table 2. Comparison of global POC fluxes (10^{15} mol/yr) and net primary production (Gt/yr) in the first oceanic layer for the year 2500. Note that phytoplankton light absorption always increases the global POC flux and net primary production.

Simulation	POC flux (10^{15} mol/yr)	Net primary production (Gt/yr)
RCP2.6	0.3794	37.42
RCP2.6-LA	0.3623	38.15
RCP4.5	0.3915	37.78
RCP4.5-LA	0.3764	38.31
RCP6.0	0.3984	37.80
RCP6.0-LA	0.3798	38.49
RCP8.5	0.4168	38.35
RCP8.5-LA	0.4121	38.67

3.1.2 Surface chlorophyll

We look at the distribution of chlorophyll at the ocean surface because this climate carbon-cycle variable directly affects the
250 heat distribution along the water column through phytoplankton light absorption. On a global scale, independently of the RCP scenario, phytoplankton light absorption leads to an increase in chlorophyll at the ocean surface (Figure 4). This increase is due to the increased global phosphate concentrations (Appendix D1) which are driven by a reduced export efficiency of organic matter and enhanced remineralization at the ocean surface (Table 2). For the RCP2.6, RCP4.5 and RCP6.0 scenarios, the global increase of chlorophyll is between 0.015 and 0.019 mgChl/m^3, representing an increase of 13-15%. These assessments
255 are slightly higher than previous estimates showing an increase between 4 and 12% (Manizza et al., 2005; Asselot et al.,

2021). However, compared to our model setup, Manizza et al. (2005) use an ocean model, neglecting any interactions between the ocean and the atmosphere. Additionally, Asselot et al. (2021) do not prescribe CO_2 emissions, neglecting the changes in chlorophyll due to climate change. The increase in chlorophyll for the RCP8.5 scenario is the smallest, with an increase of ~0.01 mgChl/m^3, representing an increase of 8%. The lower global increase of chlorophyll under RCP8.5 compared to the

260   other RCPs scenarios is due to the lower increase of chlorophyll in the mid-latitudes and upwelling regions (Figure 5).
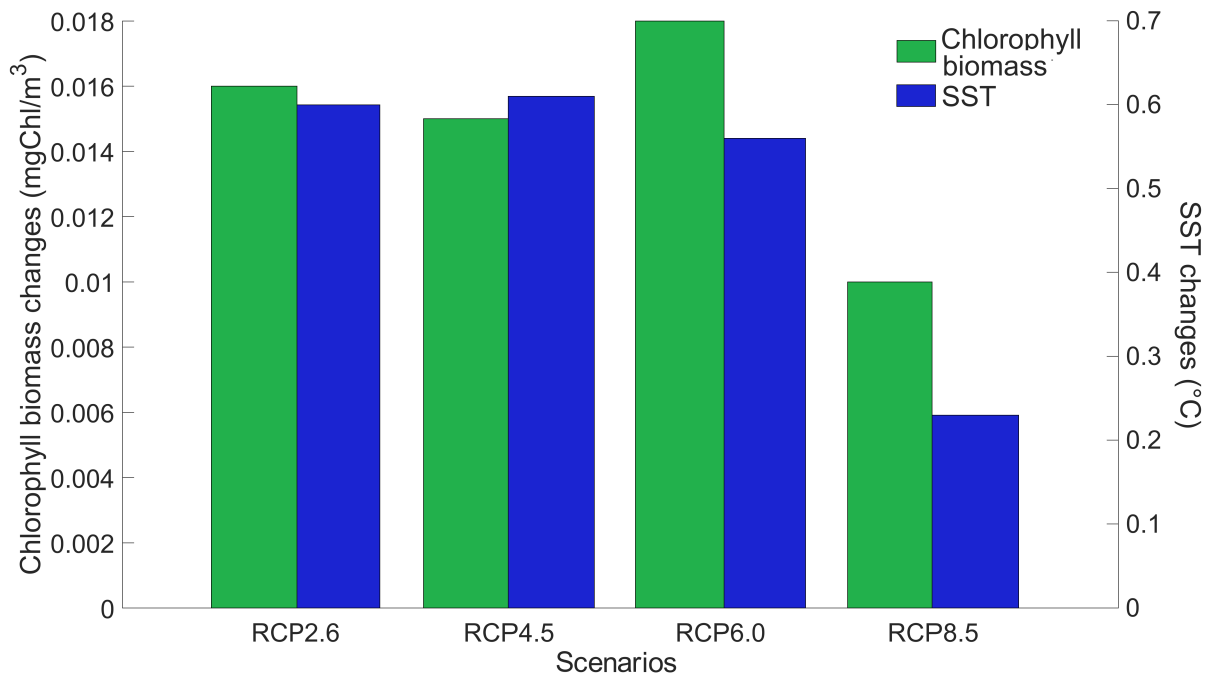
Figure 4. Globally-averaged surface chlorophyll (mgChl/m^3) and SST (°C) changes between the RCP scenarios at the year 2500. The values represent the difference between the simulation with minus without phytoplankton light absorption. Note that the y-axis scales are always positive, indicating that phytoplankton light absorption always leads to a global increase of surface chlorophyll and SST.

The regional patterns of surface chlorophyll changes due to phytoplankton light absorption are similar between the RCP scenarios (Figure 5). The largest differences in chlorophyll occur at high latitudes. Such as, between the simulations *RCP8.5-LA* and *RCP8.5*, the maximum increase of 0.4 mgChl/m^3 occurs in the northern polar region (Figure 5d). This pronounced chlorophyll response in the high latitudes is likely due to enhanced light availability due to the decrease of sea-ice. For instance,

265   the global sea-ice area decreases by 13% between *RCP8.5-LA* and *RCP8.5*, thus increasing light availability for phytoplankton growth. The upwelling and mid-latitude regions show a higher chlorophyll concentration with phytoplankton light absorption. These regional patterns are due to higher nutrient concentration at the ocean surface with phytoplankton light absorption (Appendix D1). This enhanced nutrient concentration is due to reduced export efficiency (Table 2) and higher remineralization at the ocean surface. The higher nutrient concentrations at the surface decreases the nutrient limitation and thus promoting a

270 higher phytoplankton biomass at the surface. In contrast to the upwelling regions, the nutrient-limited subtropical gyres show
no or small differences in surface chlorophyll concentrations.
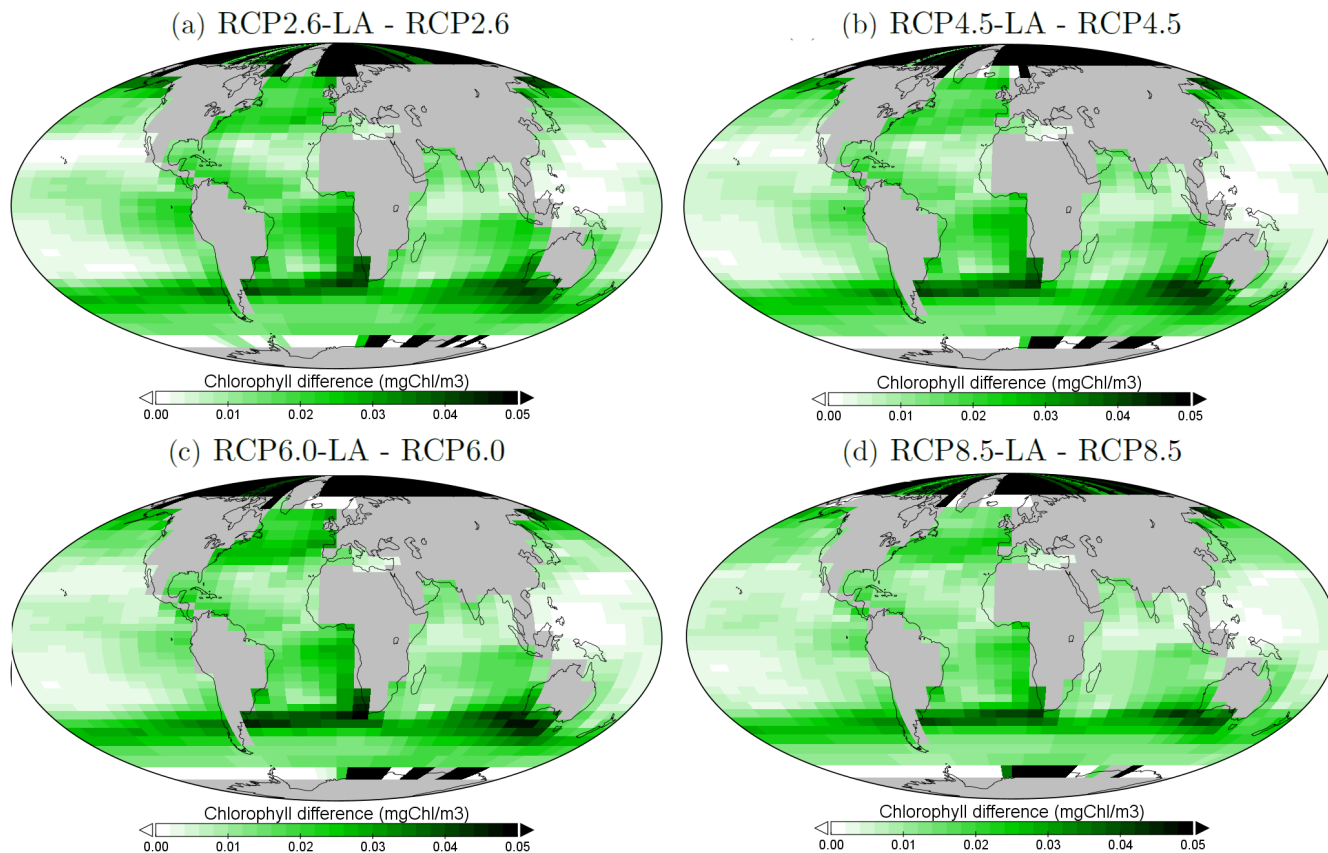
Figure 5. Surface chlorophyll changes at the year 2500 (mgChl/m^3) for the different simulations. (a) Difference between RCP2.6-LA and
RCP2.6. (b) Difference between RCP4.5-LA and RCP4.5. (c) Difference between RCP6.0-LA and RCP6.0. (d) Difference between RCP8.5-
LA and RCP8.5. The scale and color coding are identical between the four panels. Note that the scale is logarithmic and always positive.

3.1.3   Sea surface temperature

Due to changes in surface chlorophyll, we expect variations in SST. Our results highlight that under the RCP2.6, RCP4.5 and
RCP6.0 scenarios, phytoplankton light absorption increases the SST by ∼0.6°C (Figure 4). These assessments are higher than
275 previous global estimates, giving a global SST increase of 0.33-0.5°C (Wetzel et al., 2006; Patara et al., 2012; Asselot et al.,
2021). This stronger increase in SST is caused by higher increases in surface chlorophyll compared to previous assessments.
For the RCP8.5 scenario, phytoplankton light absorption only increases SST by 0.23°C. This lower increase in SST is due to
the lower increase in global surface chlorophyll under this scenario. The regional patterns of SST changes due to phytoplankton
light absorption are similar between the simulations following the RCP2.6, RCP4.5 and RCP6.0 scenarios but the magnitude

280 of changes differs (Figure 6). Under these scenarios, even though the polar regions experience a high increase in chlorophyll, they also experience the lowest increase in SST. For instance, between the simulations *RCP4.5-LA* and *RCP4.5*, the minimum increase of 0.03°C occurs in the Southern Ocean. The polar regions experience the lowest changes in SST because temperatures are buffered by latent heat through melting sea-ice and remain close to freezing. In contrast, under RCP8.5, the maximum SST increase of 0.51°C occurs in the Southern Ocean. This is due to the greatly reduced annually averaged sea ice under RCP8.5,
285 meaning that the latent heat buffering effect of melting/growing sea-ice is weaker, allowing heating of the ocean surface. The annual ice cover in the simulation RCP8.5-LA is only $5.1 \cdot 10^6$ km^2 in 2500, which compares to $25.8 \cdot 10^6$ km^2 for RCP2.6-LA. Even in the regions where small differences in surface chlorophyll occur, such as the subtropical gyres, we find high SST increases. The differing spatial patterns between chlorophyll and SST can be explained by the fact that short-lived chlorophyll is not subject to transport, while (conserved) physical quantities, such as heat, are transported by oceanic currents. Therefore,
290 heat is smoothly redistributed around the globe.
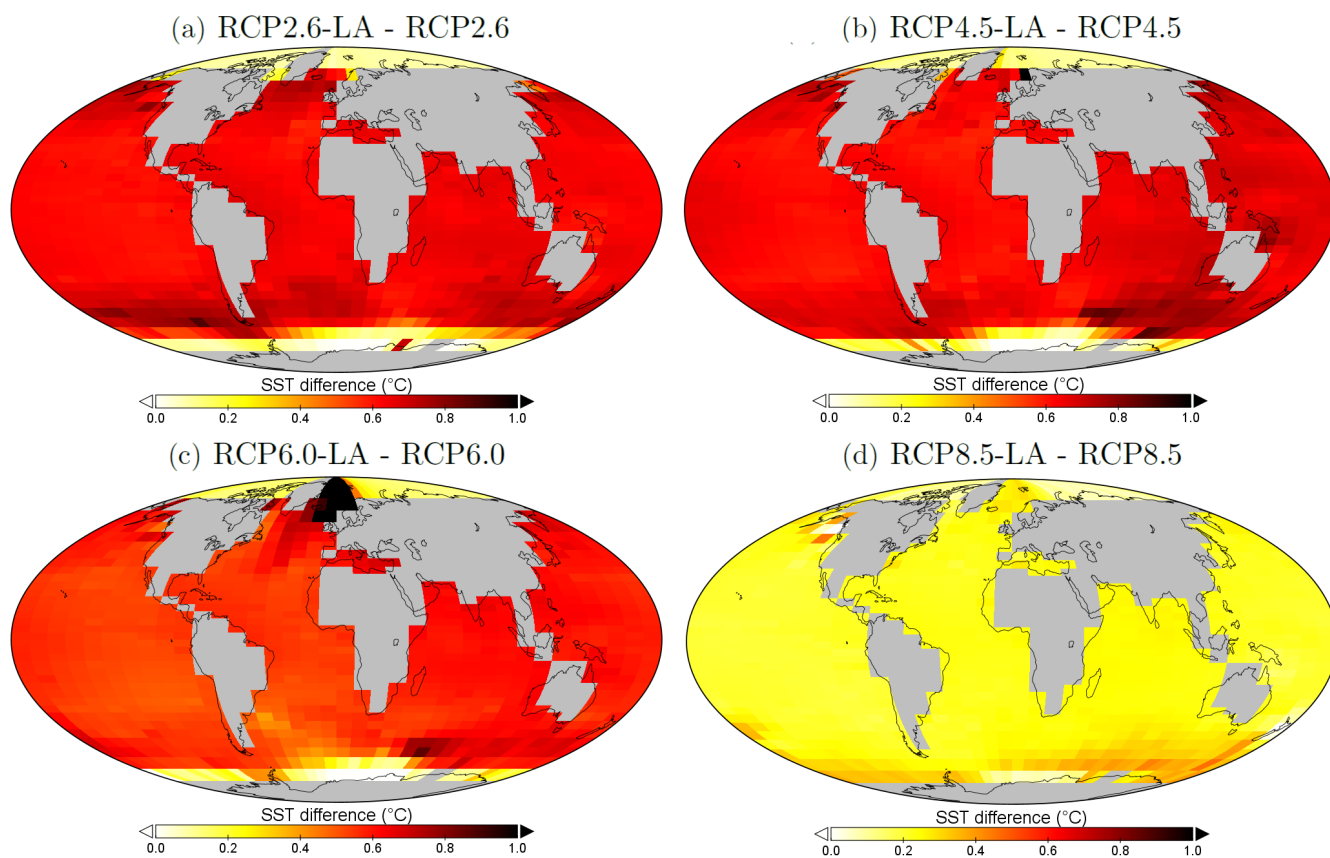
Figure 6. Sea surface temperature changes (°C) between the simulations at the year 2500. (a) Difference between RCP2.6-LA and RCP2.6. (b) Difference between RCP4.5-LA and RCP4.5. (c) Difference between RCP6.0-LA and RCP6.0. (d) Difference between RCP8.5-LA and RCP8.5. The scale and color coding are identical between the four panels. Note that the scale is always positive.

3.2 Atmospheric properties

3.2.1 Atmospheric CO_2 concentration

The atmospheric CO_2 concentrations in our simulations do not match the atmospheric concentrations of Meinshausen et al. (2011) in 2500. This is because our version of the model, with light penetrating until the sixth oceanic layer, has been tuned to get reasonable net primary production and nutrient fields but not to get future atmospheric CO_2 concentrations. As a consequence, with this configuration, the model is known to simulate low atmospheric CO_2 concentrations (Asselot et al., 2021, 2022). Because we are more interested in qualitative assessment rather than quantitative estimates, such limitation does not affect the main findings of our study. Independently of the RCP scenario, the atmospheric CO_2 concentration increases with phytoplankton light absorption (Figure 7). For the RCP2.6, RCP4.5 and RCP6.0 scenarios, phytoplankton light absorption increases the atmospheric CO_2 concentration by $\sim$20% while a previous study indicates an increase of 10% (Asselot et al., 2021). However, Asselot et al. (2021) do not prescribe CO_2 emissions, neglecting their effect on the atmospheric CO_2 concentration. For the RCP8.5 scenario, the atmospheric CO_2 concentration increases by 8% only, which is due to the lower increase in chlorophyll and SST.
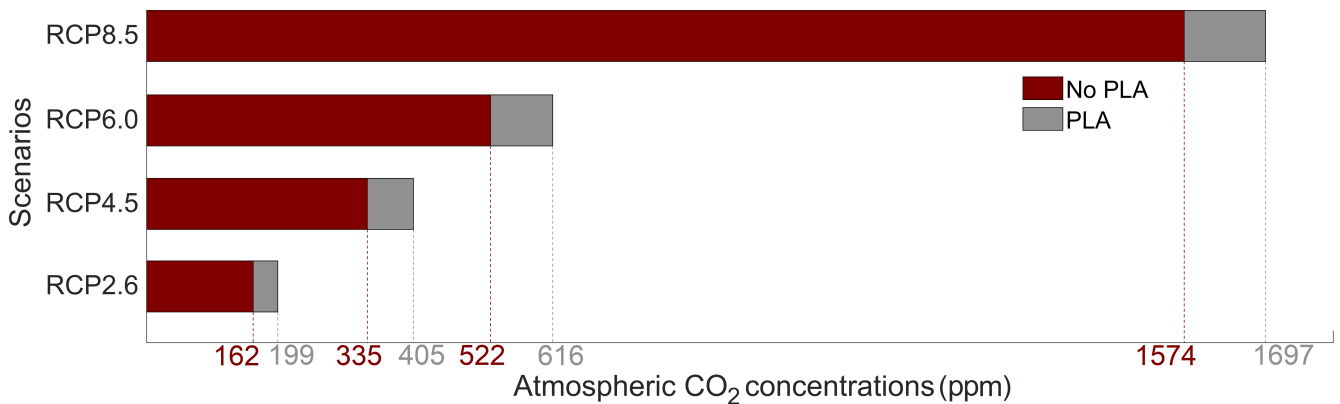
Figure 7. Atmospheric CO_2 concentrations (ppm) for the 8 simulations at year 2500. PLA stands for phytoplankton light absorption.

The increase in atmospheric CO_2 concentrations with phytoplankton light absorption is mainly due to the higher SST decreasing CO_2 solubility, and thus increasing the oceanic CO_2 outgassing (Asselot et al., 2022). Our results indicate that the reduced solubility pump enhances the ocean-to-atmosphere CO_2 flux by $\sim$10%. In contrast, the changes in the biological and carbonate pump enhance the air-sea CO_2 fluxes by $<$1%. However, the temperature dependence of solubility could not explain the changes in atmospheric CO_2 concentration in steady state, suggesting that the effect is transient. For the first three RCPs scenarios (but not RCP8.5), the change in atmospheric CO_2 concentration driven by phytoplankton light absorption follows a roughly linear dependence on the baseline concentration for that RCP (Figure 8). The rate of CO_2 uptake is roughly proportional to baseline concentration for the first three RCPs scenarios but is reduced for RCP8.5 because of the smaller effect of

phytoplankton light absorption on SST. To validate this inference, we continue our simulations for another 1000 years with no further CO_2 emissions (Appendix C1). These additional simulations indicate that CO_2 differences decrease through time, converging towards the far smaller steady-state difference previously highlighted by Asselot et al. (2021).
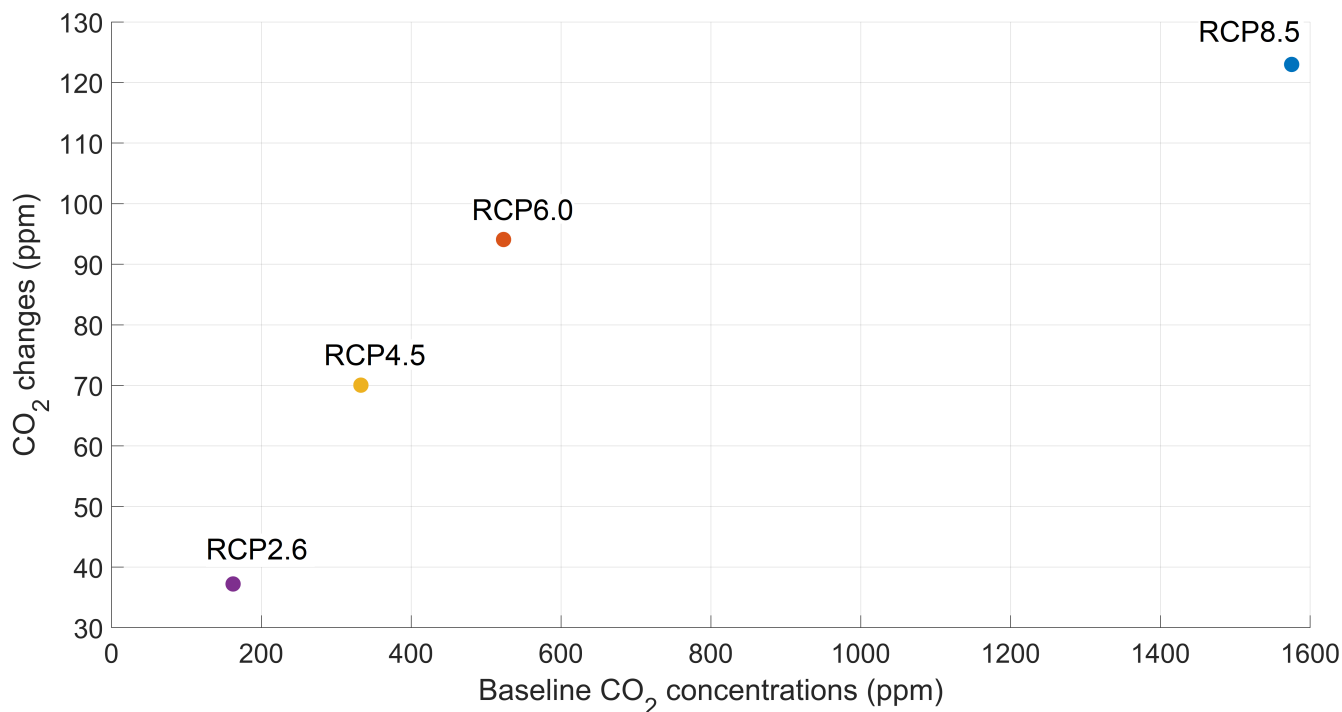
Figure 8. Phytoplankton light absorption driven CO_2 changes (ppm) under the four RCPs scenarios at the year 2500. The x-axis represents the atmospheric CO_2 concentrations of the simulations without phytoplankton light absorption.

315   3.2.2   Surface atmospheric temperature

Due to higher greenhouse gas concentrations, the atmospheric temperature increases with phytoplankton light absorption (Figure 9). For the RCP2.6, RCP4.5 and RCP6.0 scenarios, the global increase in SAT is ∼0.8°C, which is higher than previous model estimates indicating a zonally-averaged SAT increase of 0.2-0.45°C (Shell et al., 2003; Patara et al., 2012; Asselot et al., 2021). However, compared to our model setup, Shell et al. (2003) use an uncoupled ocean-atmosphere model, neglecting any interactions between the ocean and the atmosphere. Patara et al. (2012) use a constant and prescribed atmospheric CO_2 concentration for their simulations, neglecting its effect on the atmospheric temperature. Asselot et al. (2021) do not prescribe CO_2 emissions, neglecting changes in the heat budget due to climate change. With a value of 0.28°C, the increase in SAT under the RCP8.5 scenario is lower than for the other RCP scenarios. This lower value is driven by a combination of reduced SST warming and lower atmospheric CO_2 concentration changes under this RCP scenario.
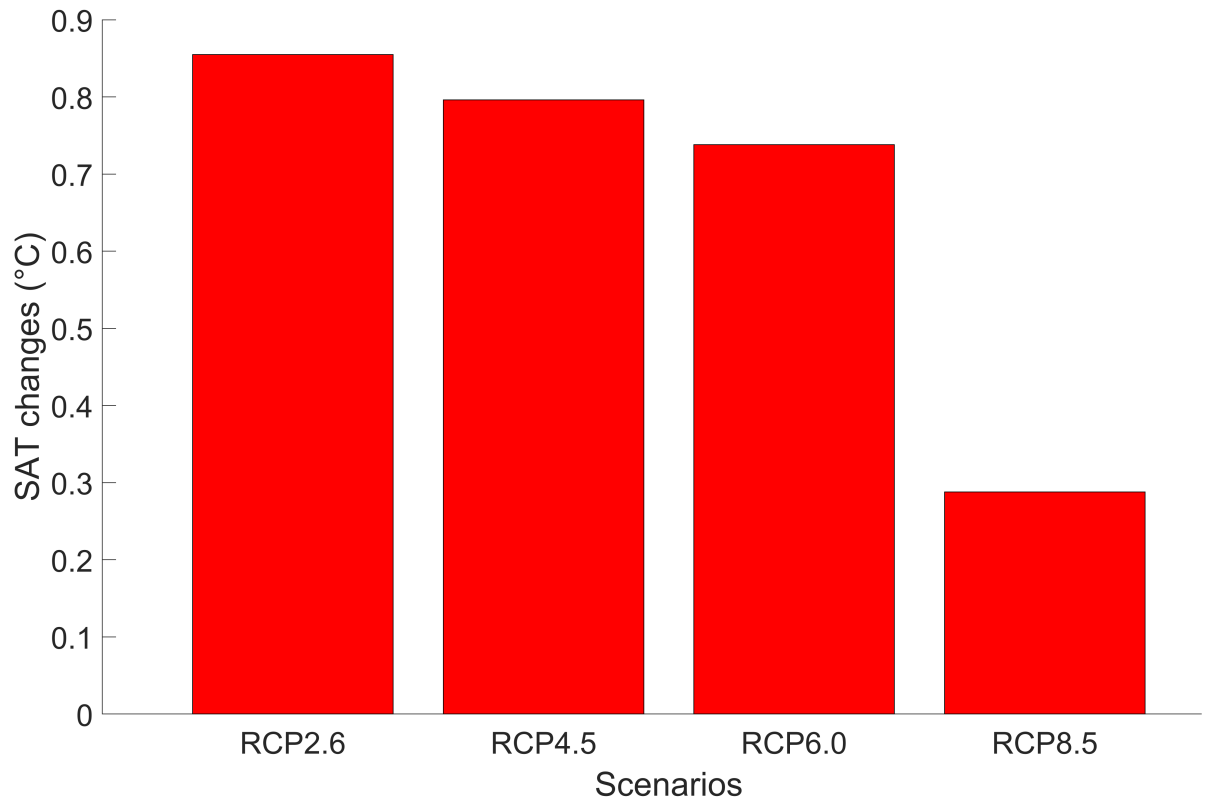
Figure 9. Globally-averaged surface atmospheric temperature (°C) changes between the RCP scenarios at the year 2500. The values represent the difference between the simulation with and without phytoplankton light absorption. Note that the y-axis scale is always positive, indicating that phytoplankton light absorption always leads to a global increase of SAT.

325   The regional patterns of SAT changes due to phytoplankton light absorption are similar among the RCP scenarios but the magnitude of changes differs (Figure 10). The polar regions experience a strong increase in SAT, with the highest values occurring in the Southern Ocean. For instance, comparing the simulations *RCP4.5-LA* and *RCP4.5*, the maximum increase of 1.6°C occurs in the Southern Ocean (Figure 10b). This maximum value is likely the result of reduced Antarctic sea-ice (lengthening of the ice-free season) and reduction of latent heat buffering. This estimate is again higher than previous local

330   estimates (Shell et al., 2003; Patara et al., 2012; Asselot et al., 2021) for the same reasons described above. Furthermore, around the rest of the globe, heat is redistributed smoothly in the atmosphere.
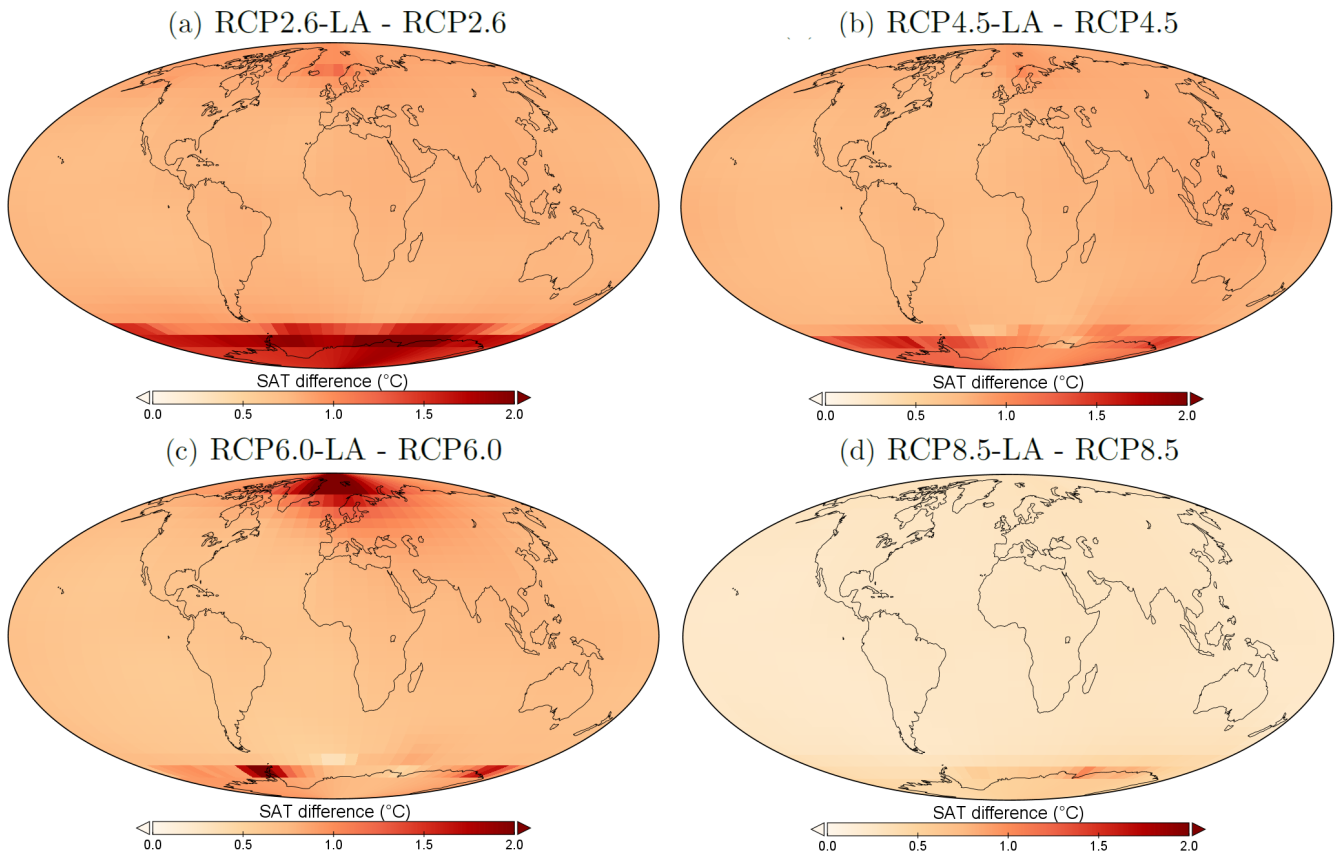
Figure 10. Surface atmospheric temperature changes (°C) between the different simulations at the year 2500. (a) Difference between RCP2.6-LA and RCP2.6. (b) Difference between RCP4.5-LA and RCP4.5. (c) Difference between RCP6.0-LA and RCP6.0. (d) Difference between RCP8.5-LA and RCP8.5. The scale and color coding are identical for the four panels. Note that the scale is always positive.

4   Discussion and conclusions

4.1   General discussion

Our results show that phytoplankton light absorption affects water temperature and nutrient concentrations. The increase in
335   surface nutrient concentrations (Appendix D1) is driven by a reduced export efficiency of organic matter and enhanced remineralization at the ocean surface (Table 2). The increased surface nutrient concentrations leads to higher surface chlorophyll, which in turn leads to a warming of the ocean surface. Furthermore, the higher CO_2 concentration associated with phytoplankton light absorption leads to an enhanced greenhouse gas effect. As a consequence, the radiative forcing increases, warming the ocean surface as well. Under the RCP2.6, RCP4.5 and RCP6.0 scenarios, phytoplankton concentration is not strongly limited by temperature. As a result the impact of phytoplankton light absorption on the climate system is similar between these

RCP scenarios. However, under the RCP8.5 scenario, the effect of phytoplankton light absorption on the climate system is reduced. This is likely due to decreasing ecosystem productivity as temperature increases (Appendix A1 and A2), caused by exponentially increasing nutrient demand and zooplankton predation, combined with sub-exponential (light limited) increases in photosynthesis. Additionally, our results demonstrate that the increase in nutrients (Table D1) is the smallest under the RCP8.5 scenario. Consequently, fewer nutrients are available, explaining partly the reduced increase of chlorophyll under this scenario. Phytoplankton concentration is thus limited by temperature and nutrient availability, leading to a weaker difference in chlorophyll between *RCP8.5-LA* and *RCP8.5* than between the other simulations (Figure 4). The response of the climate system to phytoplankton light absorption is therefore weaker under the RCP8.5 scenario. Our findings indicate that the effect of phytoplankton light absorption is smaller under high greenhouse gas emissions compared to reduced and intermediate green-house gas emissions. In agreement with Patara et al. (2012), this study indicates that a severely warmer world increases ocean clarity and slows down the warming due to phytoplankton light absorption. However, the reduced effect of phytoplankton light absorption under the RCP8.5 scenario may not be as strong if phytoplankton were able to adapt to higher temperatures in our model setup.

4.2 Limitations

For the first time, using EcoGEnIE (Ward et al., 2018), we investigate the impact of phytoplankton light absorption under prescribed CO_2 emissions following the RCP scenarios on a multi-century timescale. However, our model setup has limitations that must be overcome to improve our quantitative estimates. Most notably, our version of the model must be tuned to fit the projected atmospheric CO_2 concentrations under global warming scenarios. For instance, for the simulations following the RCP2.6 scenario, the final atmospheric CO_2 concentrations and SSTs are lower than pre-industrial levels. This is due to the negative emissions for this scenario and the underestimation of the atmospheric CO_2 concentrations with our model setup (Asselot et al., 2021, 2022). Our model setup allows for light and primary production until the sixth oceanic layer and this con-figuration has not been tuned to match projected atmospheric CO_2 concentrations, leading to an underestimation of the latter. The lower levels under the RCP2.6 scenario compared to the pre-industrial levels are not an issue for our study because we exclusively focused on the effect of phytoplankton light absorption rather than on the differences between the simulations and the pre-industrial state. Furthermore, we switch on ECOGEM and the RCP emission forcings at the same time. We know from previous work (Asselot et al., 2021), that switching on ECOGEM decreases the atmospheric CO_2 concentration, thus our simulations contain an effect of both drift and emissions. However, the drifting effect is identical between simulations and therefore balances out when comparing simulations. With our model setup we demonstrate that phytoplankton light absorption increases local SST by 0.4-1.1°C depending on the scenario considered. These estimates are lower than previous observations showing a local increase of SST by 0.95-4.5°C (Kahru et al., 1993; Capone et al., 1998; Wurl et al., 2018). The difference between our estimates and observations may in part be due to the short time scales for observations while our estimates are yearly-averaged. Our results indicate a large local increase in chlorophyll in the simulations with phytoplankton light absorption, especially in the northern polar region, likely due to reduced sea-ice and increased light availability. Additionally, if wind stress could evolve freely, we suppose that the increase in atmospheric temperature would lead to increased wind stress. As a result, upwelling dy-

namics would be altered. In our model setup, temperature significantly affects the concentration of our bulk phytoplankton. The temperature-dependent grazing that leads to increased grazing pressure as well as the temperature-dependent nutrient uptake that leads to increased nutrient limitation with increasing temperature result in a decrease in phytoplankton concentration. The response of the modeled phytoplankton might be different if we had considered different PFTs (e.g. diatoms, dinoflagellates) since their concentrations are characterized by different temperature response curves (Anderson et al., 2021). We cannot be certain that the strong phytoplankton concentration limitations in our simulations *RCP8.5-LA* and *RCP8.5* will also occur if more PFTs are considered. Depending on the model and the region of interest, the future of net primary production is highly uncertain. For instance, using a suite of nine coupled carbon-climate ESMs under the RCP8.5 scenario, Laufkötter et al. (2015) show that net primary production may increase, remain stable or decrease under global warming. Though we note that the simulations of Laufkötter et al. (2015) only went out to 2100, not to 2500 as in our extended simulations. Our results highlight that phytoplankton light absorption itself increases chlorophyll leading to more heat being trapped in the ocean surface.

4.3 Implication for Earth system models

The traditional view is that dominant carbon cycle uncertainties come from the terrestrial response to elevated atmospheric CO_2 concentrations. For instance, the net land emissions from cGEnIE over the 1858-2008 period are estimated to be likely (66% confidence) to lie in the range from 0 to 128 GtC (Holden et al., 2013). However, this work suggests that introducing biogeophysical mechanisms such as phytoplankton light absorption leads to major carbon cycle uncertainties. For instance, with our model setup, implementing phytoplankton light absorption increases the atmospheric carbon content by 79 GtC (23%) under RCP2.6 and by 258 GtC (8%) under RCP8.5, compared to the simulations without this biogeophysical mechanism. This study highlights a highly uncertain feedback on the carbon cycle that is missing from 50% of the CMIP6 models (Pellerin et al., 2020). Neglecting the effect of phytoplankton light absorption on the carbon cycle can lead to incomplete future climate projections, thus this biogeophysical mechanism should be included by default in climate models.

Code availability. The code for the model is hosted on GitHub and can be obtained by cloning or downloading: https://zenodo.org/record/5676165. The configuration file is named "RA.ECO.ra32lv.FeTDTL.36x36x32" and can be found in the directory "EcoGENIE_LA/genie-main/configs". The user-configuration files to run the experiments can be found in the directory "EcoGENIE_LA/genie-userconfigs/RA/Asselotetal_ESD". Details of the code installation and basic model configuration can be found on a PDF file (https://www.seao2.info/cgenie/docs/muffin.pdf). Finally, section 9 of the manual provides tutorials on the ECOGEM ecosystem model.

Author contributions. All authors designed and developed the concept of the study. RA performed the analysis of the model outputs with inputs from IH. RA drafted the initial version of the manuscript in collaboration with IH. All co-authors read and reviewed the final version of the manuscript.

Competing interests. The authors declare that they have no conflict of interest.

405   *Acknowledgements.* We thank two anonymous reviewers for their comments that improve the quality of the manuscript. Our special thanks go to Jana Hinners, Isabell Hochfeld, Félix Pellerin, Maike Scheffold and Laurin Steidle for their valuable comments on the early version of this manuscript. This work was supported by the Center for Earth System Research and Sustainability (CEN), University of Hamburg, and contributes to the Cluster of Excellence "CLICCS - Climate, Climatic Change, and Society".

Appendix A: Optimum net phytoplankton growth

410   To illustrate the temperature limitation, we show the relationships between SST, surface chlorophyll and dissolved phosphate.
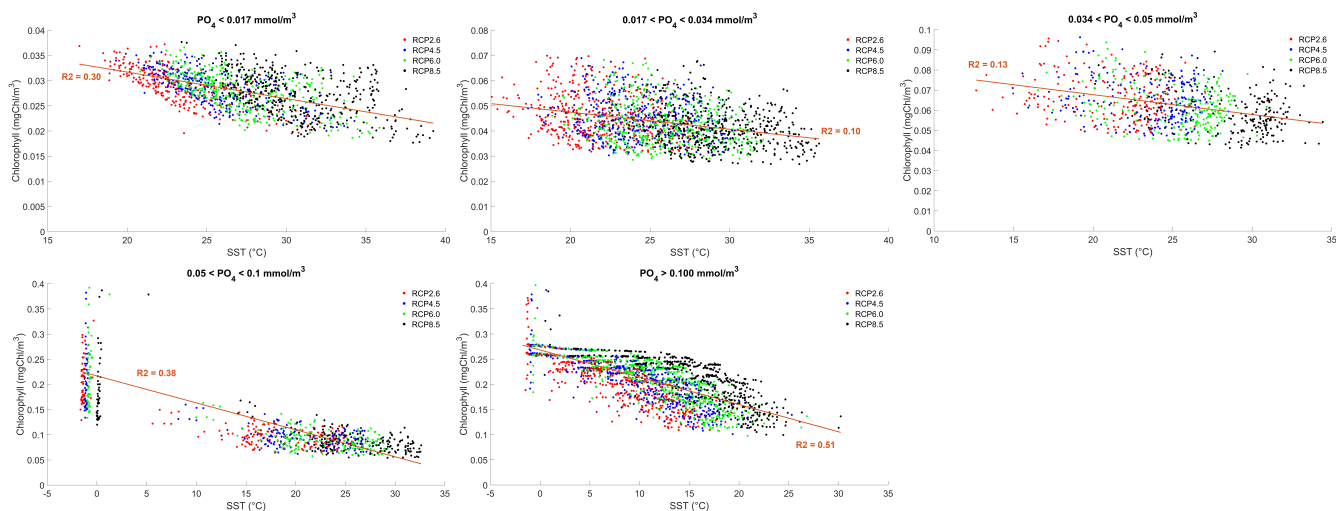
Figure A1. Effect of SST (°C) on surface chlorophyll (mgChl/m^3) for each grid cell at year 2500. The data have been divided in five panels defined by their phosphate (PO$_4$) concentrations. Red dots correspond to the simulations following the RCP2.6 scenario. Blue dots represents the simulations following the RCP4.5 scenario. Green dots represents the simulations following the RCP6.0 scenario. Black dots represents the simulations following the RCP8.5 scenario. The R-squared value represents the coefficient of determination of the linear regression model
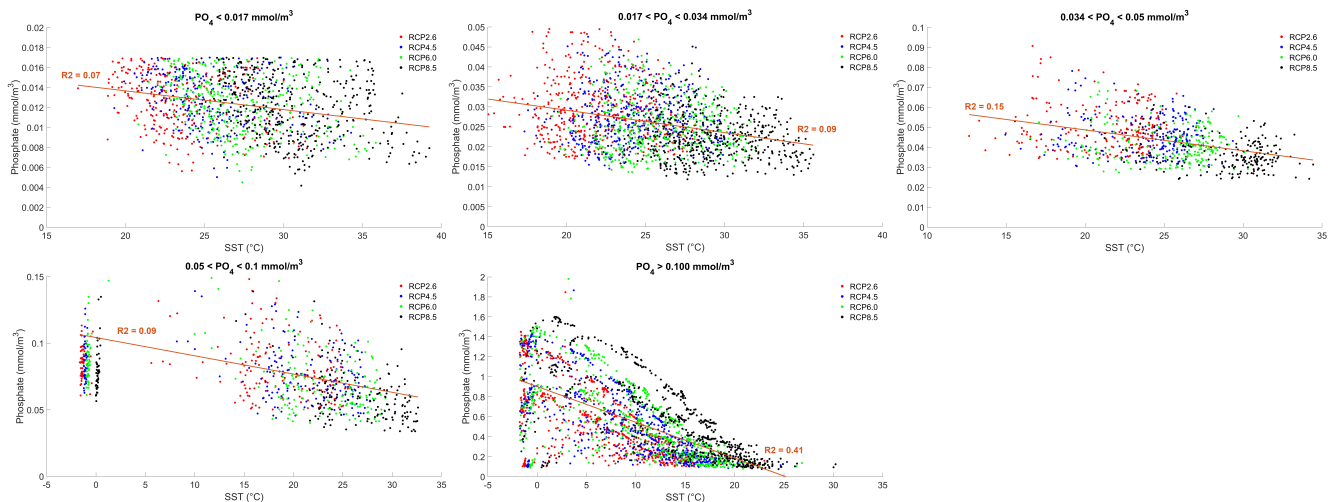
Figure A2. Effect of SST (°C) on surface phosphate (PO_4) concentrations (mmol/m^3) for each grid cell at year 2500. The data have been divided in five panels defined by their PO_4 concentrations. Red dots correspond to the simulations following the RCP2.6 scenario. Blue dots represents the simulations following the RCP4.5 scenario. Green dots represents the simulations following the RCP6.0 scenario. Black dots represents the simulations following the RCP8.5 scenario. The R-squared value represents the coefficient of determination of the linear regression model

Appendix B: Plankton functional types

We base our ecosystem community on the one described by Ward et al. (2018). We only use 2 PFTs: one phytoplankton group and one zooplankton group (Appendix B1). We show that the complexity of the ecosystem does not have an important impact on the climate system compared to the effect of phytoplankton light absorption (Asselot et al., 2021). Therefore, for simplification, we reduce the ecosystem's complexity.

Table B1. Size of the different plankton functional types (μm) used during the simulations.

PFT	Size (μm)
Phytoplankton	46.25
Zooplankton	146.15

Appendix C: Additional simulations

To investigate the substantially reduced ocean CO_2 uptake with phytoplankton light absorption, we continue our simulations for another 1000 years with no further CO_2 emissions. The difference in atmospheric CO2 concentrations between the simulations with and without phytoplankton light absorption decreases with time. This result evidences that large CO_2 differences are driven by a transient effect of reduced CO_2 uptake fluxes, consistent with reduced CO_2 solubility under phytoplankton light absorption warming.
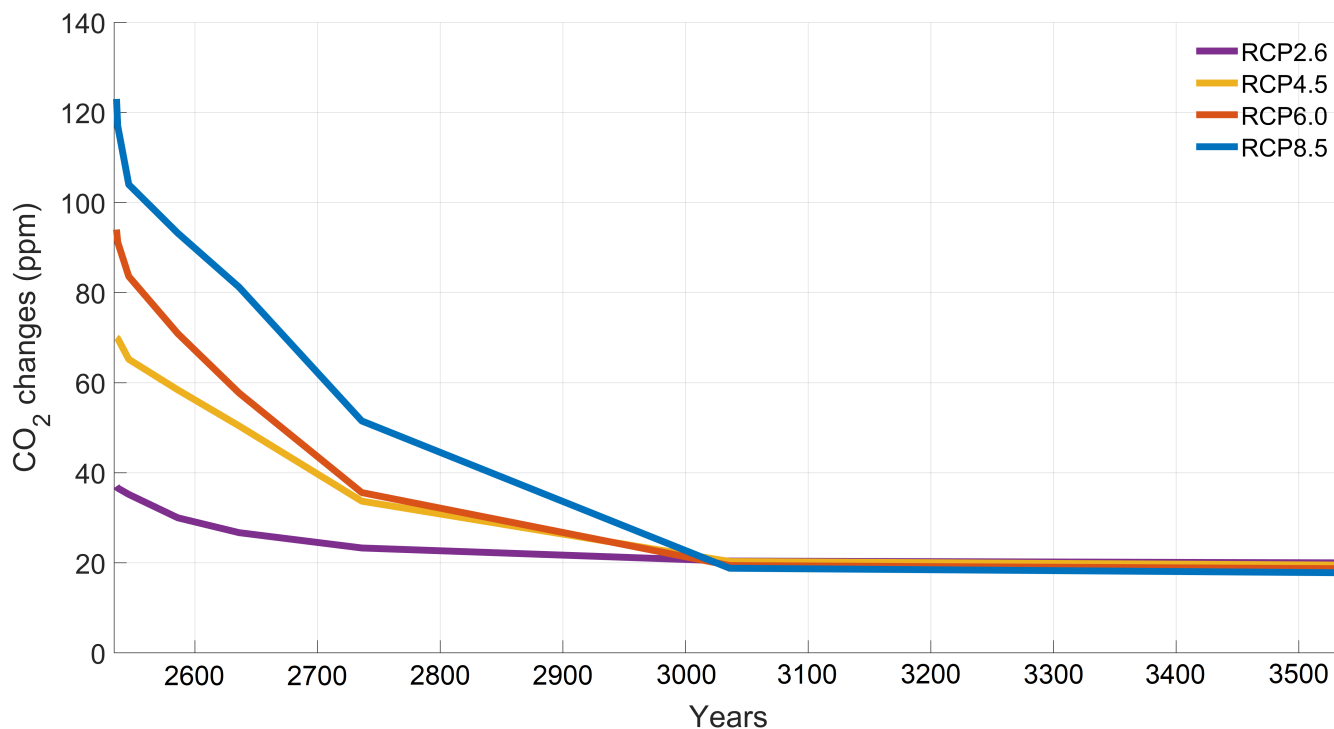
Figure C1. Difference in atmospheric CO_2 concentrations through time for the additional simulations.

Appendix D: Surface phosphate concentration

Independent of the RCP scenarios, our results evidence an increase in surface nutrients, such as phosphate. As a result, the surface chlorophyll biomass increases with phytoplankton light absorption.

Table D1. Phosphate concentration changes at the surface (mol/kg) for the different RCP scenarios at year 2500. The values represent the difference with minus without phytoplankton light absorption. The "+" symbol indicates an increase in surface PO_4 concentration.

Scenario	ΔPO_4 conc. (mol/kg)
RCP2.6	$+8.9 \cdot 10^{-8}$
RCP4.5	$+8.6 \cdot 10^{-8}$
RCP6.0	$+9.1 \cdot 10^{-8}$
RCP8.5	$+7.5 \cdot 10^{-8}$

425 Appendix E: Sea surface temperature

Table E1. Sea surface temperature (°C) for the different simulations.

Simulations	SST(°C)
RCP2.6	15.95
RCP2.6LA	16.54
RCP4.5	18.08
RCP4.5LA	18.68
RCP6.0	19.18
RCP6.0LA	19.75
RCP8.5	23.21
RCP8.5LA	23.44

References

Anderson, S., Barton, A., Clayton, S., Dutkiewicz, S., and Rynearson, T.: Marine phytoplankton functional types exhibit diverse responses to thermal change, Nature communications, 12, 1–9, 2021.

Anderson, W., Gnanadesikan, A., Hallberg, R., Dunne, J., and Samuels, B.: Impact of ocean color on the maintenance of the Pacific Cold Tongue, Geophysical Research Letters, 34, 2007.

Asselot, R., Lunkeit, F., Holden, P. B., and Hense, I.: The relative importance of phytoplankton light absorption and ecosystem complexity in an Earth system model, Journal of Advances in Modeling Earth Systems, 13, e2020MS002 110, 2021.

Asselot, R., Lunkeit, F., Holden, P. B., and Hense, I.: Climate pathways behind phytoplankton-induced atmospheric warming, Biogeosciences, 19, 223–239, 2022.

Behrenfeld, M. J. and Falkowski, P. G.: Photosynthetic rates derived from satellite–based chlorophyll concentration, Limnology and oceanography, 42, 1–20, 1997.

Boyce, D. G., Dowd, M., Lewis, M. R., and Worm, B.: Estimating global chlorophyll changes over the past century, Progress in Oceanography, 122, 163–173, 2014.

Cael, B., Bisson, K., Boss, E., Dutkiewicz, S., and Henson, S.: Global climate-change trends detected in indicators of ocean ecology, Nature, pp. 1–4, 2023.

Cameron, D. R., Lenton, T. M., Ridgwell, A. J., Shepherd, J. G., Marsh, R., and Yool, A.: A factorial analysis of the marine carbon cycle and ocean circulation controls on atmospheric CO_2, Global Biogeochemical Cycles, 19, 2005.

Capone, D. G., Subramaniam, A., Montoya, J. P., Voss, M., Humborg, C., Johansen, A. M., Siefert, R. L., and Carpenter, E. J.: An extensive bloom of the N_2-fixing cyanobacterium Trichodesmium erythraeum in the central Arabian Sea, Marine Ecology Progress Series, 172, 281–292, 1998.

Claussen, M., Mysak, L., Weaver, A., Crucifix, M., Fichefet, T., Loutre, M.-F., Weber, S., Alcamo, J., Alexeev, V., Berger, A., Calov, R., Ganopolski, A., Goosse, H., Lohmann, G., Lunkeit, F., Mokhov, I., Petoukhov, V., Stone, P., and Wang, W.: Earth system models of intermediate complexity: closing the gap in the spectrum of climate system models, Climate dynamics, 18, 579–586, 2002.

Conkright, M. E. and Levitus, S.: World Ocean Atlas 2001. Volume 4, Nutrients, 2002.

Edwards, N. R. and Marsh, R.: Uncertainties due to transport-parameter sensitivity in an efficient 3-D ocean-climate model, Climate Dynamics, 24, 415–433, 2005.

Geider, R. J., MacIntyre, H. L., and Kana, T. M.: A dynamic regulatory model of phytoplanktonic acclimation to light, nutrients, and temperature, Limnology and oceanography, 43, 679–694, 1998.

Gibbs, S. J., Bown, P. R., Ridgwell, A., Young, J. R., Poulton, A. J., and O'Dea, S. A.: Ocean warming, not acidification, controlled coccolithophore response during past greenhouse climate change, Geology, 44, 59–62, 2016.

Goldman, J. C.: Temperature effects on phytoplankton growth in continuous culture, Limnology and Oceanography, 22, 932–936, 1977.

Greene, S., Ridgwell, A., Kirtland Turner, S., Schmidt, D. N., Pälike, H., Thomas, E., Greene, L., and Hoogakker, B.: Early Cenozoic decoupling of climate and carbonate compensation depth trends, Paleoceanography and paleoclimatology, 34, 930–945, 2019.

Hense, I.: Regulative feedback mechanisms in cyanobacteria-driven systems: a model study, Marine Ecology Progress Series, 339, 41–47, 2007.

Henson, S. A., Sarmiento, J. L., Dunne, J. P., Bopp, L., Lima, I., Doney, S. C., John, J., and Beaulieu, C.: Detection of anthropogenic climate change in satellite records of ocean chlorophyll and productivity, Biogeosciences, 7, 621–640, 2010.

Hibler, W. D.: A dynamic thermodynamic sea ice model, Journal of physical oceanography, 9, 815–846, 1979.

Holden, P., Edwards, N., Müller, S., Oliver, K., Death, R., and Ridgwell, A.: Controls on the spatial distribution of oceanic $\delta^{13}C_{DIC}$,

465   Biogeosciences, 10, 1815–1833, 2013.

Holden, P. B., Edwards, N. R., Fraedrich, K., Kirk, E., Lunkeit, F., and Zhu, X.: PLASIM–GENIE v1.0: a new intermediate complexity AOGCM, Geoscientific Model Development, 9, 3347–3361, 2016.

Kahru, M., Leppanen, J.-M., and Rud, O.: Cyanobacterial blooms cause heating of the sea surface, Marine Ecology Progress Series, 101, 1–7, 1993.

470   Kvale, K. F. and Meissner, K. J.: Primary production sensitivity to phytoplankton light attenuation parameter increases with transient forcing, Biogeosciences, 14, 4767–4780, 2017.

Kwiatkowski, L., Torres, O., Bopp, L., Aumont, O., Chamberlain, M., Christian, J. R., Dunne, J. P., Gehlen, M., Ilyina, T., John, J. G., et al.: Twenty-first century ocean warming, acidification, deoxygenation, and upper-ocean nutrient and primary production decline from CMIP6 model projections, Biogeosciences, 17, 3439–3470, 2020.

475   Laufkötter, C., Vogt, M., Gruber, N., Aita-Noguchi, M., Aumont, O., Bopp, L., Buitenhuis, E. T., Doney, S. C., Dunne, J. P., Hashioka, T., Hauck, J., Hirata, T., John, J. G., Le Quere, C., Lima, I. D., Nakano, H., Seferian, R., Totterdell, I. J., Vichi, M., and Volker, C.: Drivers and uncertainties of future global marine primary production in marine ecosystem models, Biogeosciences, 12, 6955–6984, 2015.

Lewis, M. R., Cullen, J. J., and Platt, T.: Phytoplankton and thermal structure in the upper ocean: consequences of nonuniformity in chlorophyll profile, Journal of Geophysical Research: Oceans, 88, 2565–2570, 1983.

480   Mahowald, N. M., Yoshioka, M., Collins, W. D., Conley, A. J., Fillmore, D. W., and Coleman, D. B.: Climate response and radiative forcing from mineral aerosols during the last glacial maximum, pre-industrial, current and doubled-carbon dioxide climates, Geophysical Research Letters, 33, 2006.

Manizza, M., Le Quéré, C., Watson, A. J., and Buitenhuis, E. T.: Bio-optical feedbacks among phytoplankton, upper ocean physics and sea-ice in a global model, Geophysical Research Letters, 32, 2005.

485   Marsh, R., Müller, S., Yool, A., and Edwards, N.: Incorporation of the C-GOLDSTEIN efficient climate model into the GENIE framework: "eb_go_gs" configurations of GENIE, Geoscientific Model Development, 4, 957–992, 2011.

McClain, C. R., Signorini, S. R., and Christian, J. R.: Subtropical gyre variability observed by ocean-color satellites, Deep Sea Research Part II: Topical Studies in Oceanography, 51, 281–301, 2004.

Meinshausen, M., Smith, S. J., Calvin, K., Daniel, J. S., Kainuma, M., Lamarque, J.-F., Matsumoto, K., Montzka, S., Raper, S., Riahi, K.,

490   et al.: The RCP greenhouse gas concentrations and their extensions from 1765 to 2300, Climatic change, 109, 213, 2011.

Meyer, K., Ridgwell, A., and Payne, J.: The influence of the biological pump on ocean chemistry: implications for long-term trends in marine redox chemistry, the global carbon cycle, and marine animal ecosystems, Geobiology, 14, 207–219, 2016.

Moore, J. K., Doney, S. C., Kleypas, J. A., Glover, D. M., and Fung, I. Y.: An intermediate complexity marine ecosystem model for the global domain, Deep Sea Research Part II: Topical Studies in Oceanography, 49, 403–462, 2001.

495   Moss, R. H., Edmonds, J. A., Hibbard, K. A., Manning, M. R., Rose, S. K., Van Vuuren, D. P., Carter, T. R., Emori, S., Kainuma, M., Kram, T., et al.: The next generation of scenarios for climate change research and assessment, Nature, 463, 747–756, 2010.

Park, J.-Y., Kug, J.-S., Bader, J., Rolph, R., and Kwon, M.: Amplified Arctic warming by phytoplankton under greenhouse warming, Proceedings of the National Academy of Sciences, 112, 5921–5926, 2015.

Patara, L., Vichi, M., Masina, S., Fogli, P. G., and Manzini, E.: Global response to solar radiation absorbed by phytoplankton in a coupled

500   climate model, Climate dynamics, 39, 1951–1968, 2012.

Paulsen, H.: The effects of marine nitrogen-fixing cyanobacteria on ocean biogeochemistry and climate–an Earth system model perspective, Ph.D. thesis, Universität Hamburg Hamburg, 2018.

Pellerin, F., Porada, P., and Hense, I.: ESD Reviews: Evidence of multiple inconsistencies between representations of terrestrial and marine ecosystems in Earth System Models, Earth System Dynamics Discussions [preprint], pp. 1–26, 2020.

505 Polovina, J. J., Howell, E. A., and Abecassis, M.: Ocean's least productive waters are expanding, Geophysical Research Letters, 35, 2008.

Reale, M., Cossarini, G., Lazzari, P., Lovato, T., Bolzon, G., Masina, S., Solidoro, C., and Salon, S.: Acidification, deoxygenation, and nutrient and biomass declines in a warming Mediterranean Sea, Biogeosciences, 19, 4035–4065, 2022.

Reinhard, C. T., Planavsky, N. J., Ward, B. A., Love, G. D., Le Hir, G., and Ridgwell, A.: The impact of marine nutrient abundance on early eukaryotic ecosystems, Geobiology, 18, 139–151, 2020.

510 Rhee, G.-Y. and Gotham, I. J.: The effect of environmental factors on phytoplankton growth: temperature and the interactions of temperature with nutrient limitation, Limnology and Oceanography, 26, 635–648, 1981.

Richon, C., Dutay, J.-C., Bopp, L., Le Vu, B., Orr, J. C., Somot, S., and Dulac, F.: Biogeochemical response of the Mediterranean Sea to the transient SRES-A2 climate change scenario, Biogeosciences, 16, 135–165, 2019.

Ridgwell, A., Hargreaves, J., Edwards, N. R., Annan, J., Lenton, T. M., Marsh, R., Yool, A., and Watson, A.: Marine geochemical data
515 assimilation in an efficient Earth system Model of global biogeochemical cycling, Biogeosciences, 4, 87–104, 2007.

Schlunegger, S., Rodgers, K. B., Sarmiento, J. L., Ilyina, T., Dunne, J. P., Takano, Y., Christian, J. R., Long, M. C., Frölicher, T. L., Slater, R., et al.: Time of emergence and large ensemble intercomparison for ocean biogeochemical trends, Global biogeochemical cycles, 34, e2019GB006 453, 2020.

Semtner, A. J.: A model for the thermodynamic growth of sea ice in numerical investigations of climate, Journal of Physical Oceanography,
520 6, 379–389, 1976.

Shell, K., Frouin, R., Nakamoto, S., and Somerville, R.: Atmospheric response to solar radiation absorbed by phytoplankton, Journal of Geophysical Research: Atmospheres, 108, 2003.

Sonntag, S.: Modeling biological-physical feedback mechanisms in marine systems, Ph.D. thesis, Universität Hamburg Hamburg, 2013.

Stockey, R. G., Pohl, A., Ridgwell, A., Finnegan, S., and Sperling, E. A.: Decreasing Phanerozoic extinction intensity as a consequence of
525 Earth surface oxygenation and metazoan ecophysiology, Proceedings of the National Academy of Sciences, 118, 2021.

Tagliabue, A., Kwiatkowski, L., Bopp, L., Butenschön, M., Cheung, W., Lengaigne, M., and Vialard, J.: Persistent Uncertainties in Ocean Net Primary Production Climate Change Projections at Regional Scales Raise Challenges for Assessing Impacts on Ecosystem Services, Frontiers in Climate, p. 149, 2021.

Thompson, S. L. and Warren, S. G.: Parameterization of outgoing infrared radiation derived from detailed radiative calculations, Journal of
530 Atmospheric Sciences, 39, 2667–2680, 1982.

Trenberth, K. E.: A global ocean wind stress climatology based on ECMWF analyses, NCAR Tech. note, 93, 1989.

Wanninkhof, R.: Relationship between wind speed and gas exchange over the ocean, Journal of Geophysical Research: Oceans, 97, 7373–7382, 1992.

Ward, B. A., Wilson, J. D., Death, R., Monteiro, F. M., Yool, A., and Ridgwell, A.: EcoGEnIE 1.0: plankton ecology in the cGEnIE Earth
535 system model, Geoscientific Model Development, 11, 4241–4267, 2018.

Weaver, A. J., Eby, M., Wiebe, E. C., Bitz, C. M., Duffy, P. B., Ewen, T. L., Fanning, A. F., Holland, M. M., MacFadyen, A., Matthews, H. D., et al.: The UVic Earth System Climate Model: Model description, climatology, and applications to past, present and future climates, Atmosphere-Ocean, 39, 361–428, 2001.

Wetzel, P., Maier-Reimer, E., Botzet, M., Jungclaus, J., Keenlyside, N., and Latif, M.: Effects of ocean biology on the penetrative radiation in a coupled climate model, Journal of Climate, 19, 3973–3987, 2006.

Wilson, J., Monteiro, F., Schmidt, D., Ward, B., and Ridgwell, A.: Linking marine plankton ecosystems and climate: A new modeling approach to the warm early Eocene climate, Paleoceanography and Paleoclimatology, 33, 1439–1452, 2018.

Wurl, O., Bird, K., Cunliffe, M., Landing, W. M., Miller, U., Mustaffa, N. I. H., Ribas-Ribas, M., Witte, C., and Zappa, C. J.: Warming and inhibition of salinization at the ocean's surface by cyanobacteria, Geophysical research letters, 45, 4230–4237, 2018.

Zickfeld, K., Eby, M., Weaver, A. J., Alexander, K., Crespin, E., Edwards, N. R., Eliseev, A. V., Feulner, G., Fichefet, T., Forest, C. E., et al.: Long-term climate change commitment and reversibility: an EMIC intercomparison, Journal of Climate, 26, 5782–5809, 2013.